Supplementary Material

Appendix A Description of input channels for the narrow resonance search

The selected input channels include all those motivated by the multi-lepton anomalies. Thus, in addition to inclusive searches, we focus on the production of S in association with leptons, (b-)jets, and/or missing energy, while excluding other channels from the ATLAS analysis in Ref. [1], such as the $\gamma\gamma + \gamma$ channel, even if they show excesses. To conduct this study, we leverage CMS and ATLAS analyses of the Standard Model Higgs-boson, which inherently explore potential resonances in their side bands, covering a mass range up to 180 GeV. However, due to some analyses ending at 160 GeV and to avoid interference with the SM Higgs-boson resonance, we restrict our analysis to the mass range between 140 GeV and 155-160 GeV, as appropriate. This specific mass range is both suggested by and consistent with the observed multi-lepton anomalies.

The description of each input channel considered in this analysis is listed below.

$\boldsymbol{S(\rightarrow \gamma\gamma, Z\gamma)}$ **(*Phys.Rev.D* 108, 115031)**: The first combination, published in Ref. [2], includes data reported up until 2021, but with an update to the $Z\gamma$ channel:

- $S(\rightarrow \gamma\gamma) + E^T_{\rm miss}$: In these channels, m_S is reconstructed from the invariant mass of $\gamma\gamma$, and S is produced in association with $E^T_{\rm miss}$. The data is taken from Fig. 6 in Ref. [3] and Fig. 3 in Ref. [4]).
- $S(\rightarrow b\bar{b}) + E^T_{\rm miss}$: m_S is reconstructed from the invariant mass of $b\bar{b}$, and S is produced in association with $E^T_{\rm miss}$ originating from the decay of S to the invisible final states. The data is taken from Fig. 5 in Ref. [5].
- $S(\rightarrow \gamma\gamma) + b$-jet: m_S decays to two photons and is produced in association with b quarks (which, in the 2HDM+S model, could originate from S but also from h if $H \rightarrow Sh$ is non-negligible). The data is obtained from Fig. 2 (top-right) in Ref. [6] and Fig. 2 in Ref. [7].
- $S(\rightarrow \gamma\gamma) + W, Z$: S decays to two photons and is produced in association with a W or a Z boson. The corresponding data is taken from Ref. [8] and Fig. 9 c) and d) in Ref. [9].
- $S \rightarrow \gamma\gamma$ (inclusive): Here m_S is reconstructed from the invariant mass of the photon pair while the search is quasi-inclusive. However, vector boson fusion, W, and Z as well as top quark-associated production are excluded. Note that there is no veto on missing energy, but that this channel covers only a very tiny phase space of the quasi-inclusive final search. (see Fig. 15 (top-left) in Ref. [8] and Fig. 9 a) of Ref. [9]).

- $S(\to Z(\to \ell^+\ell^-)\gamma) + 1\ell, jj$: We use Fig. 3 top-left in Ref. [10][1] and Fig. 3 Bottom-right in Ref. [10]. This supersedes the previously used input from Fig. 5 in Ref. [11].
- $S(\to \gamma\gamma)$ + 2b-jets: The mass of S is reconstructed from the invariant mass of di-photon where S is produced in association with two b-jets. We use Fig. 8(a) in Ref. [12].

In the second combination, we have considered the following channels which published after 2021, in addition to the previously mentioned channels:

- $\boldsymbol{S(\to \gamma\gamma)+ \geq 4j}$: Here m_S corresponds to the invariant mass of the di-photon pair which is produced in association with at least 4 jets (Fig. 2 a) in Ref. [1]).
- $\boldsymbol{S(\to WW^*) + E^T_{\mathbf{miss}}}$: The CMS and ATLAS analyses of the SM Higgs-boson decaying to a pair of W bosons are recast and combined. Here we use the 0-jet category for which the dominant contribution from the simplified model described above arises from $H \to S(\to WW^*)S^*(\to E^T_{\text{miss}})$. Other final states from associated production have very small jet veto survival probability. For ATLAS, we have used the data from Fig. 11 of Ref. [13] and for CMS the m_T distributions ($p_{T2} < 20\,\text{GeV}$ and $p_{T2} > 20\,\text{GeV}$) of Fig. 1 of Ref. [14].
- $\boldsymbol{S(\to \gamma\gamma)+\geq (1\ell + 1b-\mathbf{jet})}$: S decays to two photons and is produced in association with at least one electron or muon (ℓ) and at least one tagged b-jet. The relevant experimental data are taken from Fig. 5 a) in Ref. [1].

Finally, in addition to these two combinations, we have considered a recent study from the ATLAS collaboration in this analysis:

- $\boldsymbol{S(\to \gamma\gamma) + \ell, \tau, 2(\ell, \tau)}$: Here, the mass of S is reconstructed from the invariant mass of di-photons which is produced in association with one lepton (μ or e) or tauon or two leptons or tauons. The relevant experimental results are taken from Fig.7 in Ref. [15].

Appendix B Object and Event Selection

The selection criteria, applied to each channel used in this analysis, are tabulated in Table Table B1. Here, γ_1 and γ_2 denote the leading and sub-leading photons ordered by p_T respectively. The ΔE_T^{miss} is the difference between the E_T^{miss} calculated from the vertex selected by the neural network and the E_T^{miss} calculated from the hardest vertex. Lastly, $\Delta R \equiv \sqrt{(\Delta\eta)^2 + (\Delta\phi)^2}$ where ϕ is the azimuthal angle around z-axis and η is the pseudorapidity, and y is the rapidity.

Appendix C Individual Fits for the input channels in search of the narrow resonance

In this section, we present the individual fits of the different channels considered in this analysis. We analyze the CMS and ATLAS studies to search for new scalars in the mass range between 140 GeV and 170 GeV. In each category, we model the background

[1] Following the simplified model, we chose the two jet category that is inconsistent with the Vector Boson Fusion production mechanism.

Channel	Selection Criteria
$S(\to\gamma\gamma)+\tau$ [15]	$N_\tau=1$, $N_\gamma=2$, $N_{b-\text{jet}}=0$, $E_T^{\text{miss}}>35\,\text{GeV}$, $105\,\text{GeV}>m_{\gamma\gamma}>160\,\text{GeV}$ $E_T(\gamma_1)>35\,\text{GeV}$, $\gamma_1: p_T/m_{\gamma\gamma}>0.35$, $\gamma_2: p_T/m_{\gamma\gamma}>0.25$
$S(\to\gamma\gamma)+\ell$ [15]	$N_\tau=0$, $N_\gamma=2$, $N_{b-\text{jet}}=0$ $E_T^{\text{miss}}>35$ GeV, $\gamma\gamma+eE_T(\gamma_1)>35\,\text{GeV}$, $105\,\text{GeV}>m_{\gamma\gamma}>160\,\text{GeV}$, $\gamma_1: p_T/m_{\gamma\gamma}>0.35$, $\gamma_2: p_T/m_{\gamma\gamma}>0.25$
$S(\to\gamma\gamma)+2(\ell,\tau)$ [15]	$N_\ell+N_\tau=2$, $N_\gamma=2$, $N_{b-\text{jet}}=0$ $E_T^{\text{miss}}>35\,\text{GeV}$, $E_T(\gamma_1)>35\,\text{GeV}$, $m_{2(\ell,\tau)}>12\,\text{GeV}$, $105\,\text{GeV}>m_{\gamma\gamma}>160\,\text{GeV}$, $\gamma_1: p_T/m_{\gamma\gamma}>0.35$, $\gamma_2: p_T/m_{\gamma\gamma}>0.25$
$S(\to\gamma\gamma)+b\bar{b}$ [12]	$N_\gamma=2$, $N_{b-\text{jet}}=2$, $N_{\ell=e,\mu}=0$, $E_T^{\text{miss}}>35\,\text{GeV}$, $E_T(\gamma_1)>35\,\text{GeV}$, $m_{2(\ell,\tau)}>12\,\text{GeV}$, $105\,\text{GeV}>m_{\gamma\gamma}>160\,\text{GeV}$, $\gamma_1: p_T/m_{\gamma\gamma}>0.35$, $\gamma_2: p_T/m_{\gamma\gamma}>0.25$ Fewer than six central ($\lvert\eta\rvert<2.5$) jets are present.
$S(\to\gamma\gamma)+\geq 1\ell+1b-$jet [1]	$N_{\ell=e,\mu}\geq 1$, $N_{b-\text{jet}}\geq 1$, $\gamma: p_T>22\,\text{GeV}$, $\lvert\eta\rvert<2.37$, $1.37<\lvert\eta\rvert<1.52$ $e: p_T>10\,\text{GeV}$, $\lvert\eta\rvert<2.47$, $1.37<\lvert\eta\rvert<1.52$ $\mu: p_T>10\,\text{GeV}$, $\lvert\eta\rvert<2.7$, $105\,\text{GeV}>m_{\gamma\gamma}>160\,\text{GeV}$, $\gamma_1: p_T>35\,\text{GeV}$, $p_T/m_{\gamma\gamma}>0.35$, $\gamma_2: p_T>25\,\text{GeV}$, $p_T/m_{\gamma\gamma}>0.25$
$S(\to\gamma\gamma)+\geq 4$ jet [1]	$N_{\text{jet}}\geq 4$, $\lvert N_{\text{jet}}\rvert<2.5$, $\gamma: p_T>22\,\text{GeV}$, $\lvert\eta\rvert<2.37$, $1.37<\lvert\eta\rvert<1.52$ $105\,\text{GeV}>m_{\gamma\gamma}>160\,\text{GeV}$, jet $: p_T>25\,\text{GeV}$, $\gamma_1: p_T>35\,\text{GeV}$, $p_T/m_{\gamma\gamma}>0.35$, $\gamma_2: p_T>25\,\text{GeV}$, $p_T/m_{\gamma\gamma}>0.25$
$S(\to Z(\to\ell^+\ell^-)\gamma)+1\ell, jj$ [10]	$\gamma: \lvert\eta\rvert<2.5$, $p_T>15\,\text{GeV}$, $p_T/m_{\ell^+\ell^-\gamma}>0.14$, $e: p_T>25$ (15) GeV for leading (subleading), $\lvert\eta\rvert<2.5$, $\mu: p_T>20$ (10) GeV for leading (subleading), $\lvert\eta\rvert<2.4$, jet $: p_T>30\,\text{GeV}$, $\lvert\eta\rvert<4.7$ $105\,\text{GeV}>m_{\ell^+\ell^-\gamma}>170\,\text{GeV}$, $m_{\ell^+\ell^-\gamma}+m_{\ell^+\ell^-}>185\,\text{GeV}$, $m_{\ell^+\ell^-}>50\,\text{GeV}$
$S(\to\gamma\gamma)+E_{\text{miss}}^T$ (ATLAS) [3]	$\gamma: \lvert\eta\rvert<2.37$, $1.37<\lvert\eta\rvert<1.52$, $\gamma_1: E_T/m_{\gamma\gamma}>0.35$, $\gamma_2: E_T/m_{\gamma\gamma}>0.25$, $105\,\text{GeV}>m_{\gamma\gamma}>160\,\text{GeV}$, $E_T^{\text{miss}}>90\,\text{GeV}$, $\Delta E_T^{\text{miss}}<30\,\text{GeV}$
$S(\to\gamma\gamma)+E_{\text{miss}}^T$ (CMS) [4]	$\gamma: \lvert\eta\rvert<1.44$ or $1.57<\lvert\eta\rvert<2.50$, $\gamma_1: p_T>30\,\text{GeV}$, $\gamma_2: p_T>20\,\text{GeV}$, $m_{\gamma\gamma}>95\,\text{GeV}$
$S(\to\gamma\gamma)+W,Z$ (CMS) [8]	Photons, Electrons, or neutral hadrons with $p_T>15\,\text{GeV}$, No more than two charged particles ($p_T>1.6\,\text{GeV}$ and $\lvert\eta\rvert<2.2$), $\gamma_1: p_T>35\,\text{GeV}$, $\gamma_2: p_T>25\,\text{GeV}$, $\gamma: \lvert\eta\rvert<2.5\,\text{GeV}$, except $1.44<\lvert\eta\rvert<1.57$, jets $: p_T>25\,\text{GeV}$, $\lvert\eta\rvert<4.7$, ΔR(jet,γ) >0.4, $100\,\text{GeV}<m_{\gamma\gamma}<180\,\text{GeV}$
$S(\to\gamma\gamma)+W,Z$ (ATLAS) [9]	$\gamma: \lvert\eta\rvert<2.37\,\text{GeV}$, except $1.37<\lvert\eta\rvert<1.52$, $\gamma_1: p_T/m_{\gamma\gamma}>0.35$, $\gamma_2: p_T/m_{\gamma\gamma}>0.25$, jets $: p_T>25\,\text{GeV}$, $\lvert y\rvert<4.4$, e $: p_T>10\,\text{GeV}$, $\lvert\eta\rvert<2.47$ $\mu: p_T>10\,\text{GeV}$, $\lvert\eta\rvert<2.7$ Category 1: $p_T^{W,Z}<75\,\text{GeV}$ Category 2: $75\,\text{GeV}\leq p_T^{W,Z}<150$ GeV Category 3: $150\,\text{GeV}<p_T^{W,Z}<250\,\text{GeV}$ with 0 -jet or ≥ 1 -jet Category 4: $p_T^{W,Z}>250\,\text{GeV}$ $105\,\text{GeV}>m_{\gamma\gamma}>160\,\text{GeV}$, $\Delta R(e,\gamma\gamma)>0.4$, $\Delta R(\text{jets},\gamma\gamma)>0.4$, $\Delta R(\text{jets},e)>0.2$, $\Delta R(\mu,\gamma\gamma)>0.4$, $\Delta R(\mu,\text{jets})>0.4$
$S(\to\gamma\gamma)\geq 1t$ (ATLAS) [6]	$\gamma_1: p_T>35\,\text{GeV}$, $p_T/m_{\gamma\gamma}>0.35$, $\gamma_2: p_T>25\,\text{GeV}$, $p_T/m_{\gamma\gamma}>0.25$ $105\,\text{GeV}>m_{\gamma\gamma}>160\,\text{GeV}$, $N_{\text{jet}}\geq 1$, $p_T^{\text{jet}}>25\,\text{GeV}$, containing 1 b-jet Region 1 (“Lep” region) : $N_{e,\mu}\geq 1$, $p_T^{e,\mu}>15\,\text{GeV}$, Region 2 (“Had” region) : at least two additional jets with $p_T>25\,\text{GeV}$ and no selected lepton
$S(\to\gamma\gamma)\geq 1t$ (CMS) [7]	$\gamma_1: p_T/m_{\gamma\gamma}>1/3$, $\gamma_2: p_T/m_{\gamma\gamma}>1/4$ $100\,\text{GeV}>m_{\gamma\gamma}>180\,\text{GeV}$, Region 1 (“Lep” region) : $N_{\text{jet}}\geq 1$, $p_T^{\text{jet}}>25\,\text{GeV}$, $\lvert\eta\rvert<2.4$, $N_{e,\mu}\geq 1$, $p_T^e>10\,\text{GeV}$, $p_T^\mu>5\,\text{GeV}$, Region 2 (“Had” region) : at least 3 jets, at least 1 b-jet and no selected lepton

Table B1 Selection criteria applied to each channel to form the signal pre-selection regions.

using the background function:

$$f(m;b,\{a\}) = (1-m)^b (m)^{a_0+a_1\log(m)}\,, \tag{C1}$$

where $a_{0,1}$ and b are free parameters (different for each category) and m is the invariant mass of the distribution, e.g. the di-photon mass. The choice of this particular functional form to model the background is not important for our study. [2]

We incorporate a double-sided Crystal Ball function to the background, parameterized by Equation C1, to model the signal contribution:

$$N \cdot \begin{cases} e^{-t^2/2} & \text{if } -\alpha_{\text{Low}} \leq t \leq \alpha_{\text{High}} \\ \dfrac{e^{-0.5\alpha_{\text{Low}}^2}}{\left[\frac{\alpha_{\text{Low}}}{n_{\text{Low}}}\left(\frac{n_{\text{Low}}}{\alpha_{\text{Low}}}-\alpha_{\text{Low}}-t\right)\right]^{n_{\text{Low}}}} & \text{if } t < -\alpha_{\text{Low}} \\ \dfrac{e^{-0.5\alpha_{\text{High}}^2}}{\left[\frac{\alpha_{\text{High}}}{n_{\text{High}}}\left(\frac{n_{\text{High}}}{\alpha_{\text{High}}}-\alpha_{\text{High}}+t\right)\right]^{n_{\text{High}}}} & \text{if } t > \alpha_{\text{High}}. \end{cases} \tag{C2}$$

Here N is a normalization parameter, $t = (m - m_S)/\sigma_{CB}$ where σ_{CB} is the width of the Gaussian part of the function, m is the invariant mass of the distribution and m_S the mass of the new scalar.

Now, we illustratively point towards a prominent narrow structure consistent with the detector resolution around 152 GeV.

Each graph in Figure C6 combines the spectra from the LHC experiments for the same final states by re-weighting using signal-over-background yields (N_S/N_B).

Here, N_S represents the signal yield within a mass window $\pm 2\sigma_{\text{res}}$ at the peak; σ_{res} is the di-photon invariant mass resolution embedded into a Crystal Ball function used to model the resonance, and N_B represents the corresponding background events within this range.

The mass spectra are shown for the data sets before (upper left) and after (lower left) 2021. The graph on the right shows the weighted addition of the data sets considered here. A prominent narrow structure consistent with the detector resolution around 152 GeV can be appreciated. However, it is important to note that this graph is not applicable for the significance calculation around 152 GeV.

Appendix D Fiducial Cross-sections of the 152 GeV Candidate

In this section, we tabulate the individual significance and the fiducial cross section (σ_F) of each of the channels considered in this analysis. The cross-sections are measured in two ways: across the entire kinematic range and inside a fiducial phase space that is as near as possible to the experimental measurement range. The fiducial phase space is established using stable particles produced by Monte Carlo (MC) generators, which are then used to create reconstructed objects such as primary leptons, jets, and missing transverse momentum. The advantage of fiducial cross-section measurements is a significant reduction in the amount of the applied acceptance corrections, resulting

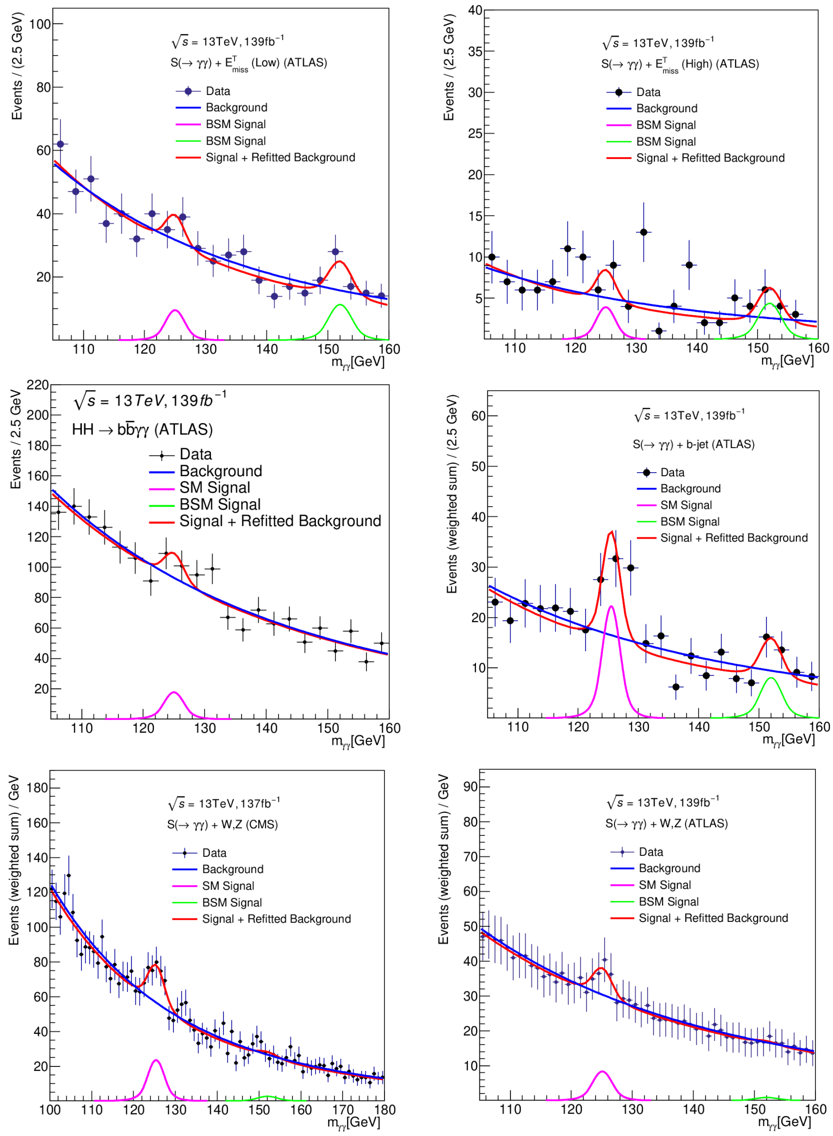

Fig. C1 Diagrams showing the fit to background obtained within the SM, the SM Higgs signal, and the NP signal with the refitted background for five different categories. The data displayed in the last three plots corresponds to a weighted sum (see refs. [9, 16, 17] for further details).

in lower systematic errors. The fiducial cross-section is defined as follows:

$$\sigma_F = \frac{\text{No. of Signal events } (N_{\text{Sig}})}{\text{Efficiency}(\epsilon) \times \text{Integrated Luminosity}(\mathcal{L})} \tag{D3}$$

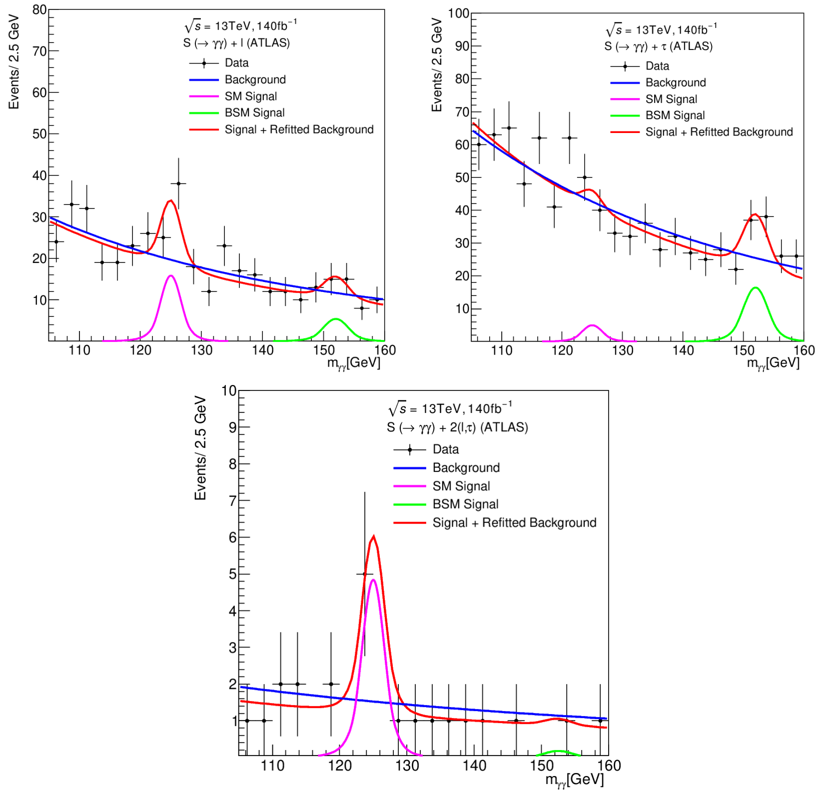

Fig. C2 Diagrams showing the fit to background obtained within the SM, the SM Higgs signal, and the NP signal with the refitted background for $S(\to\gamma\gamma)+\ell$, $S(\to\gamma\gamma)+\tau$ and $S(\to\gamma\gamma)+2(\ell,\tau)$ categories from ref.[15].

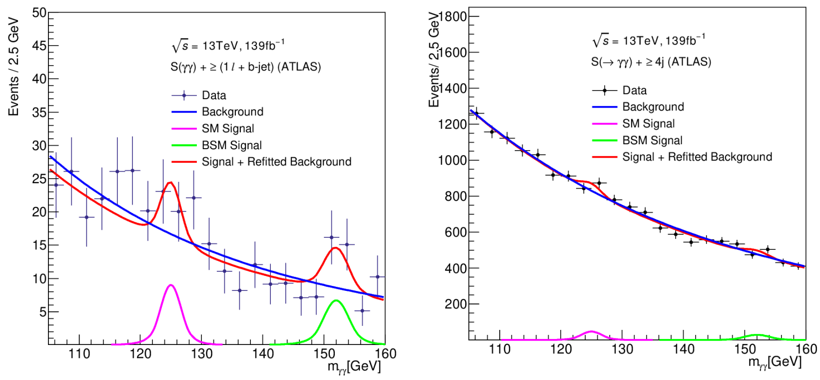

Fig. C3 Diagrams showing the fit to background obtained within the SM, the SM Higgs signal, and the NP signal with the refitted background for $S(\to\gamma\gamma)+\geq(1\ell+1b\text{-jet})$ [1] and $S(\to\gamma\gamma)+\geq 4$ jet [1] categories.

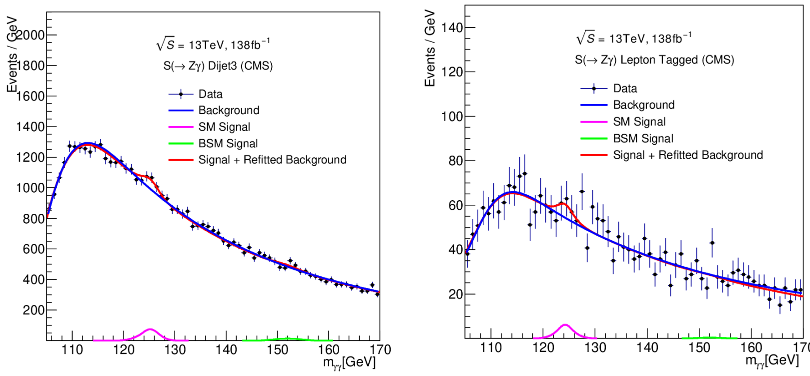

Fig. C4 Diagrams showing the fit to background obtained within the SM, the SM Higgs signal, and the NP signal with the refitted background for two different $S(\rightarrow Z\gamma)$ categories from ref. [10]

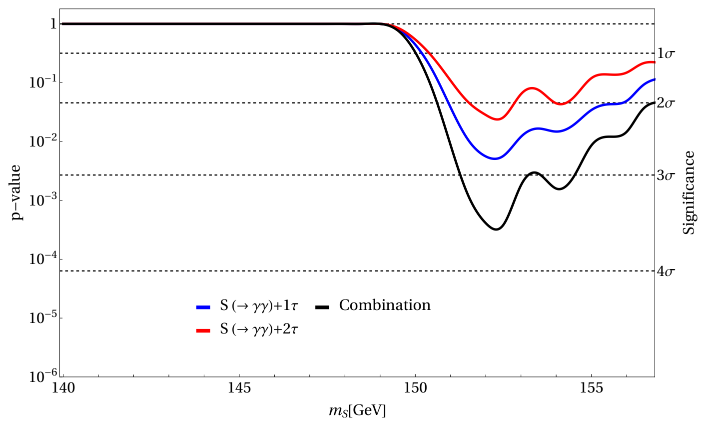

Fig. C5 The p-values of the $S(\rightarrow \gamma\gamma) + 1\tau$ and $S(\rightarrow \gamma\gamma) + 2\tau$ channels with their combination and the corresponding local significance. The best fit is obtained around 152 GeV with a local significance of 3.55σ.

Channel	Efficiency (%)
$\gamma\gamma$	60 [15]
τ	80 [15]
$\ell(e, \mu)$	88 [18, 19]
b-jet	40-70 [20]
$Z(\rightarrow \ell\ell)\gamma$	20-31 [11, 21]

Table D2 The efficiency for different channels used in this analysis.

Where N_{sig} denotes the number of signal events, ϵ defines the efficiency of different decay modes (mentioned in Table D2), and $\mathcal{L}$ is the integrated Luminosity.

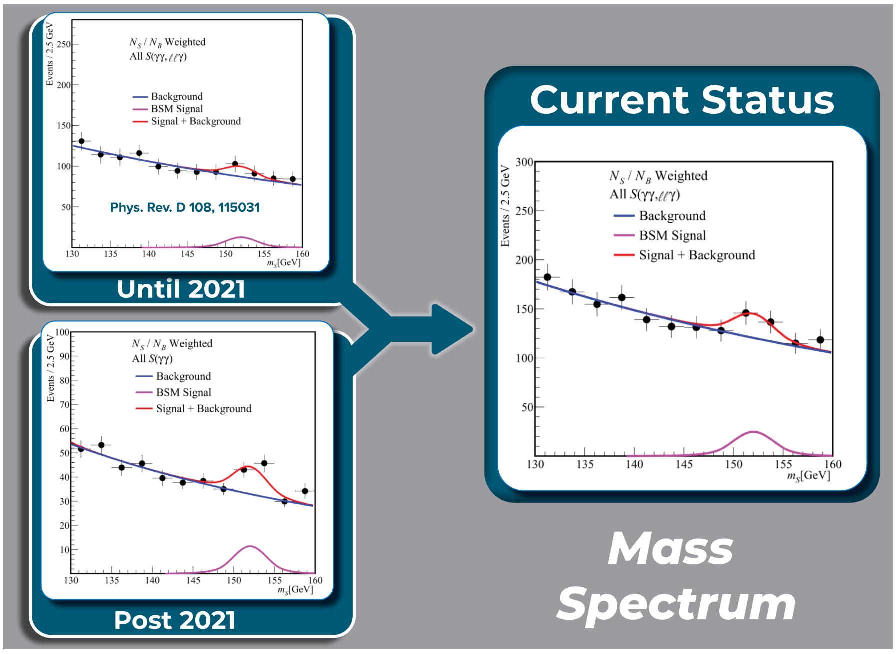

Fig. C6 The illustrative representation of the $\gamma\gamma$ and $Z\gamma$ mass spectra (see text).

Channel	N_{Sig}	Significance	σ_F in fb
$S(\to \gamma\gamma) + \tau$	32.67 $\pm$ 11.49	3.56	0.49 $\pm$ 0.17
$S(\to \gamma\gamma) + \ell$	10.72 $\pm$ 7.45	1.76	0.14 $\pm$ 0.08
$S(\to \gamma\gamma) + 2(\ell, \tau)$	0.43 $\pm$ 1.31	0.24	0.004 $\pm$ 0.01
$S(\to \gamma\gamma) + \geq 1\ell + 1b$-jet	13.30 $\pm$ 6.16	2.41	0.24 $\pm$ 0.11
$S(\to \gamma\gamma) + \geq 4$ jet	57.98 $\pm$ 35.30	1.46	0.80 $\pm$ 0.42
$S(\to Z(\to \ell^+\ell^-)\gamma) + jj$	88.61 $\pm$ 58.75	1.24	2.16 $\pm$ 1.37
$S(\to Z(\to \ell^+\ell^-)\gamma) + 1\ell$	2.49 $\pm$ 15.48	0.14	0.12 $\pm$ 0.41
$S(\to \gamma\gamma) + b-$jet	14.07 $\pm$ 6.64	2.49	0.22 $\pm$ 0.10
$S(\to \gamma\gamma) + E^T_{\text{miss}}$ (Low)	21.10 $\pm$ 7.54	2.82	0.25 $\pm$ 0.09
$S(\to \gamma\gamma) + E^T_{\text{miss}}$ (High)	8.19 $\pm$ 3.68	2.53	0.10 $\pm$ 0.04
$S(\to \gamma\gamma) + W, Z$ (CMS)	15.68 $\pm$ 14.75	0.96	0.19 $\pm$ 0.18
$S(\to \gamma\gamma) + W, Z$ (ATLAS)	4.12 $\pm$ 12.55	0.35	0.06 $\pm$ 0.17

Table D3 Fiducial Cross section for different channels used in search of the narrow resonance.

References

[1] Aad, G., *et al.*: Model-independent search for the presence of new physics in events including $H \to \gamma\gamma$ with $\sqrt{s} = 13$ TeV pp data recorded by the ATLAS detector at the LHC. JHEP **07**, 176 (2023) https://doi.org/10.1007/JHEP07(2023)176 arXiv:2301.10486 [hep-ex]

[2] Crivellin, A., Fang, Y., Fischer, O., Bhattacharya, S., Kumar, M., Malwa, E., Mellado, B., Rapheeha, N., Ruan, X., Sha, Q.: Accumulating evidence for the

associated production of a new Higgs boson at the LHC. Phys. Rev. D **108**(11), 115031 (2023) https://doi.org/10.1103/PhysRevD.108.115031 arXiv:2109.02650 [hep-ph]

[3] Aad, G., *et al.*: Search for dark matter in events with missing transverse momentum and a Higgs boson decaying into two photons in pp collisions at $\sqrt{s} = 13$ TeV with the ATLAS detector. JHEP **10**, 013 (2021) https://doi.org/10.1007/JHEP10(2021)013 arXiv:2104.13240 [hep-ex]

[4] Sirunyan, A.M., *et al.*: Search for dark matter produced in association with a Higgs boson decaying to $\gamma\gamma$ or $\tau^+\tau^-$ at $\sqrt{s} = 13$ TeV. JHEP **09**, 046 (2018) https://doi.org/10.1007/JHEP09(2018)046 arXiv:1806.04771 [hep-ex]

[5] Aad, G., *et al.*: Measurements of WH and ZH production in the $H \to b\bar{b}$ decay channel in pp collisions at 13 TeV with the ATLAS detector. Eur. Phys. J. C **81**(2), 178 (2021) https://doi.org/10.1140/epjc/s10052-020-08677-2 arXiv:2007.02873 [hep-ex]

[6] Aad, G., *et al.*: CP Properties of Higgs Boson Interactions with Top Quarks in the $t\bar{t}H$ and tH Processes Using $H \to \gamma\gamma$ with the ATLAS Detector. Phys. Rev. Lett. **125**(6), 061802 (2020) https://doi.org/10.1103/PhysRevLett.125.061802 arXiv:2004.04545 [hep-ex]

[7] Sirunyan, A.M., *et al.*: Measurements of $\mathrm{t\bar{t}}H$ Production and the CP Structure of the Yukawa Interaction between the Higgs Boson and Top Quark in the Diphoton Decay Channel. Phys. Rev. Lett. **125**(6), 061801 (2020) https://doi.org/10.1103/PhysRevLett.125.061801 arXiv:2003.10866 [hep-ex]

[8] Sirunyan, A.M., *et al.*: Measurements of Higgs boson production cross sections and couplings in the diphoton decay channel at $\sqrt{\mathrm{s}} = 13$ TeV. JHEP **07**, 027 (2021) https://doi.org/10.1007/JHEP07(2021)027 arXiv:2103.06956 [hep-ex]

[9] Aad, G., et al.: ATLAS Collaboration, "Measurement of the properties of Higgs boson production at $\sqrt{s}$=13 TeV in the $H \to \gamma\gamma$ channel using 139 fb^{-1} of pp collision data with the ATLAS experiment, ATLAS-CONF-2020-026. ATLAS-CONF-2020-026 (2020)

[10] Tumasyan, A., *et al.*: Search for Higgs boson decays to a Z boson and a photon in proton-proton collisions at $\sqrt{s} = 13$ TeV. JHEP **05**, 233 (2023) https://doi.org/10.1007/JHEP05(2023)233 arXiv:2204.12945 [hep-ex]

[11] Sirunyan, A.M., *et al.*: Search for the decay of a Higgs boson in the $\ell\ell\gamma$ channel in proton-proton collisions at $\sqrt{s} = 13$ TeV. JHEP **11**, 152 (2018) https://doi.org/10.1007/JHEP11(2018)152 arXiv:1806.05996 [hep-ex]

[12] Aad, G., *et al.*: Search for Higgs boson pair production in the two bottom quarks plus two photons final state in pp collisions at $\sqrt{s} = 13$ TeV with the

ATLAS detector. Phys. Rev. D **106**(5), 052001 (2022) https://doi.org/10.1103/PhysRevD.106.052001 arXiv:2112.11876 [hep-ex]

[13] Aad, G., *et al.*: Measurements of Higgs boson production by gluon-gluon fusion and vector-boson fusion using $H \rightarrow WW^* \rightarrow e\nu\mu\nu$ decays in pp collisions at $\sqrt{s} = 13$ TeV with the ATLAS detector. Phys. Rev. D **108**, 032005 (2023) https://doi.org/10.1103/PhysRevD.108.032005 arXiv:2207.00338 [hep-ex]

[14] Tumasyan, A., *et al.*: Measurements of the Higgs boson production cross section and couplings in the W boson pair decay channel in proton-proton collisions at $\sqrt{s} = 13 TeV$. Eur. Phys. J. C **83**(7), 667 (2023) https://doi.org/10.1140/epjc/s10052-023-11632-6 arXiv:2206.09466 [hep-ex]

[15] Aad, G., *et al.*: Search for non-resonant Higgs boson pair production in final states with leptons, taus, and photons in pp collisions at $\sqrt{s} = 13$ TeV with the ATLAS detector. JHEP **08**, 164 (2024) https://doi.org/10.1007/JHEP08(2024)164 arXiv:2405.20040 [hep-ex]

[16] Aad, G., *et al.*: CP Properties of Higgs Boson Interactions with Top Quarks in the $t\bar{t}H$ and tH Processes Using $H \rightarrow \gamma\gamma$ with the ATLAS Detector. Phys. Rev. Lett. **125**(6), 061802 (2020) https://doi.org/10.1103/PhysRevLett.125.061802 arXiv:2004.04545 [hep-ex]

[17] Sirunyan, A.M., *et al.*: Measurements of Higgs boson production cross sections and couplings in the diphoton decay channel at $\sqrt{\mathrm{s}} = 13$ TeV. JHEP **07**, 027 (2021) https://doi.org/10.1007/JHEP07(2021)027 arXiv:2103.06956 [hep-ex]

[18] Aad, G., *et al.*: Electron and photon performance measurements with the ATLAS detector using the 2015–2017 LHC proton-proton collision data. JINST **14**(12), 12006 (2019) https://doi.org/10.1088/1748-0221/14/12/P12006 arXiv:1908.00005 [hep-ex]

[19] Aad, G., *et al.*: Muon reconstruction and identification efficiency in ATLAS using the full Run 2 pp collision data set at $\sqrt{s} = 13$ TeV. Eur. Phys. J. C **81**(7), 578 (2021) https://doi.org/10.1140/epjc/s10052-021-09233-2 arXiv:2012.00578 [hep-ex]

[20] Bhattacharya, S.: Efficiency measurement of b-tagging algorithms developed by the CMS experiment. In: Meeting of the APS Division of Particles and Fields (2011)

[21] Aad, G., *et al.*: A search for the $Z\gamma$ decay mode of the Higgs boson in pp collisions at $\sqrt{s} = 13$ TeV with the ATLAS detector. Phys. Lett. B **809**, 135754 (2020) https://doi.org/10.1016/j.physletb.2020.135754 arXiv:2005.05382 [hep-ex]